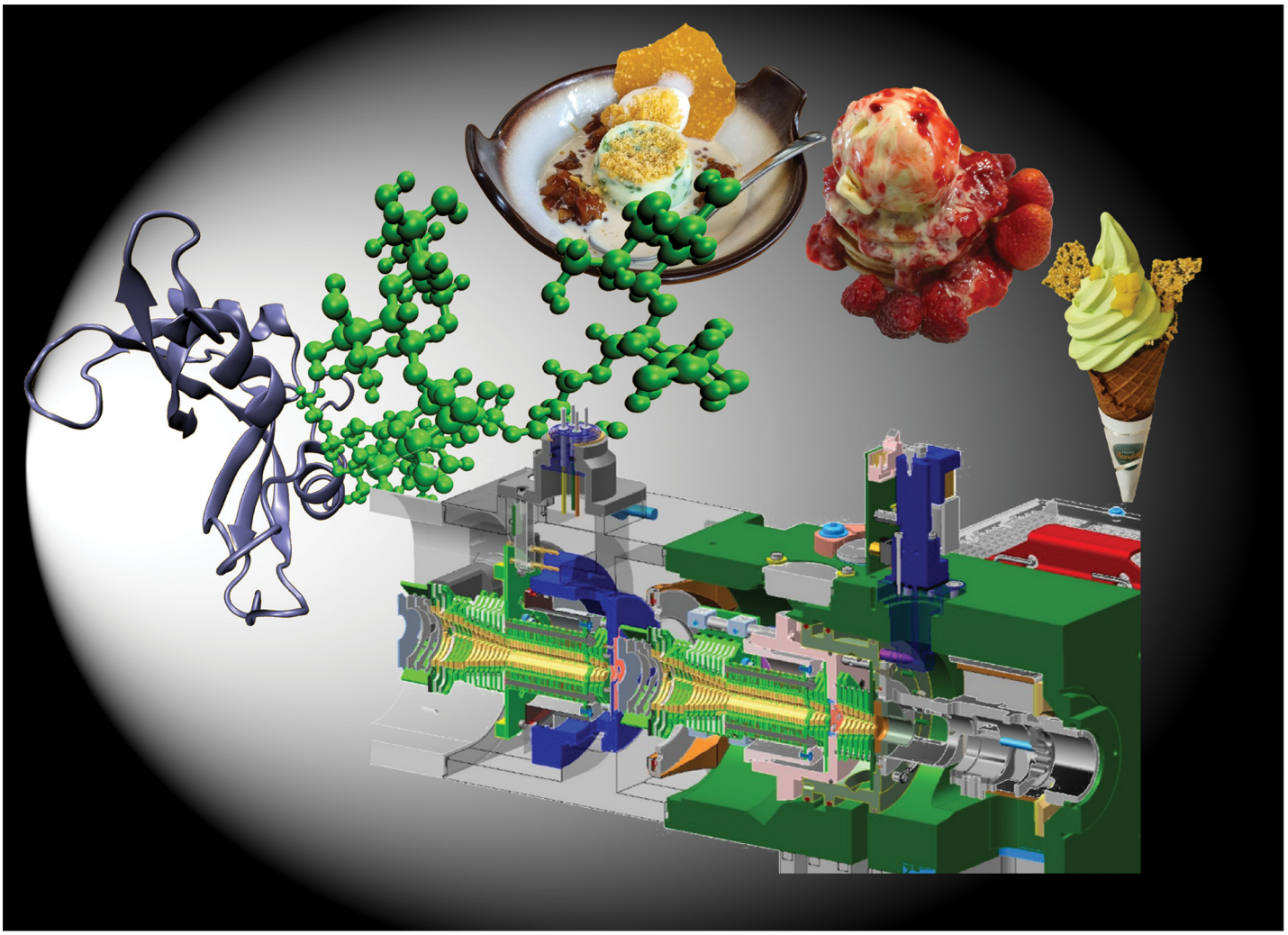

Showcasing research from Dr Liu's laboratory, Department of Chemistry and Biochemistry, Florida State University, Tallahassee/Florida, USA.

Differential melting voltage by tandem-trapped ion mobility spectrometry: glycan structure influences glycoprotein stability

Glycoproteins represent a major portion of the human proteome, comprising roughly 50–70% of all proteins. Profiling the full spectrum of protein glycoforms is critical to understanding their cellular functions. We developed the differential melting voltage approach using tandem-ion mobility/tandem-mass spectrometry to correlate the stability of individual glycoforms with their molecular characteristics. We applied this method to study Ribonuclease B and discovered that, in addition to glycan mass and protein size, the glycan structure also contributes to regulating glycoform stability.

Image reproduced by permission of Fanny Caroline Liu from *RSC Chem. Biol.*, 2025, **6**, 1711.

As featured in:

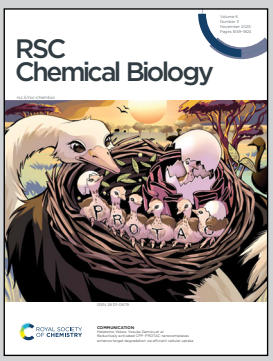

See Fanny C. Liu *et al.*, *RSC Chem. Biol.*, 2025, **6**, 1711.

ROYAL SOCIETY OF CHEMISTRY

rsc.li/rsc-chembio

Registered charity number: 207890

RSC Chemical Biology

ROYAL SOCIETY OF CHEMISTRY

COMMUNICATION

View Article Online
View Journal | View Issue

Cite this: *RSC Chem. Biol.*, 2025, 6, 1711

Received 19th May 2025,
Accepted 19th August 2025

DOI: 10.1039/d5cb00127g

rsc.li/rsc-chembio

Differential melting voltage by tandem-trapped ion mobility spectrometry: glycan structure influences glycoprotein stability

Mengqi Chai, [a] Christian Bleiholder [ab] and Fanny C. Liu *[a]

Profiling the full spectrum of protein glycoforms is critical to understanding their functional roles. We developed the differential melting voltage approach using tandem-ion mobility/tandem-mass spectrometry and applied it to study Ribonuclease B glycoforms. Our results indicate that, in addition to glycan mass and intact protein size, the glycan structure plays a role in regulating the stability of Ribonuclease B.

Glycoproteins encompass approximately 50–70% of all human proteins.[1,2] As such, glycoproteins regulate many cellular processes, including protein folding, cell signalling pathways, and immune response.[2,3] A glycoprotein typically exists as an ensemble of many variants (glycoforms), which differ in the occupancy of the glycosylation sites (macroheterogeneity) and the composition of the attached glycans (microheterogeneity).[4] The covalently attached glycan residues influence the structural heterogeneity and dynamics, which might alter the biophysical properties and function of the glycoprotein. For example, distinct glycoforms of IgG antibodies vary in their binding affinities towards Fcγ receptors of immune cells, thereby triggering either protective or pathogenic immune responses.[5] Aberrant IgG glycoforms have been shown to interfere with cellular signalling pathways, leading to autoimmune diseases. Thus, addressing how distinct glycosylation alters biophysical properties and function of proteins is of immense importance.

Solution-phase methodologies such as NMR spectroscopy, differential scanning calorimetry (DSC), and differential scanning fluorimetry (DSF) offer insights into the structures, dynamics, and stability of proteins. However, these methods struggle to resolve the heterogeneity of biological systems such as glycoproteins. This constraint primarily stems from the difficulty in separating distinct protein glycoforms. One possible approach to overcome this limitation is to generate distinct, highly homogeneous protein glycoforms to examine their function and stability.[6] However, this method is typically associated with tremendous efforts in the synthesis, purification, and analysis when investigating the full set of glycoforms of the glycoprotein of interest.

Mass spectrometry, with its high sensitivity, resolution, and throughput, serves as a powerful technique to study glycoproteins. Native mass spectrometry is commonly employed in glycoproteomics to detect lower charge states of intact glycoproteins, facilitating the identification of closely related glycoforms with subtle mass differences.[7] In conjunction with ion mobility/mass spectrometry, collisional activation has been successfully applied in glycomics and glycoproteomics.[8–10] For instance, collision-induced unfolding (CIU) has been utilized to examine the stability of antibody glycoforms.[8,11] The CIU method visualizes changes in a protein's cross section as a two-dimensional heatmap, referred to as the CIU fingerprint. However, the complexity of these fingerprints may make it less straightforward to directly correlate glycoform stability with molecular characteristics such as mass, shape, or glycan structure. Therefore, representing the stability of individual glycoforms obtained from collisional activation measurements using a single, measurable metric would be highly valuable for glycoprotein identification and characterization.

Tandem-trapped ion mobility spectrometry coupled to tandem-mass spectrometry (Tandem-TIMS),[12,13] is a novel technique that enables non-ensemble measurements. Tandem-TIMS comprises two sequential trapped ion mobility spectrometry (TIMS) analysers (Fig. 1A). At the interface between TIMS-1 and TIMS-2, ions with a specific conformation can be selectively transmitted and activated using an elevated electric field.[14–17] As such, Tandem-TIMS/tandem-MS can interrogate ions of specific mass and conformation. Using this non-ensemble approach, we recently showed that the conformational heterogeneity of the humanised IgG1k NIST monoclonal antibody is not regulated by differential glycosylation.[18] This finding highlights the potential of Tandem-TIMS for examining complex, heterogeneous systems such as glycoproteins.

In this study, we developed a Tandem-TIMS-based assay to characterize the relative stability of distinct protein glycoforms, termed differential melting voltage. In analogy to DSC and DSF,

[a] *Department of Chemistry and Biochemistry, Florida State University, 102 Varsity Way, Tallahassee, Florida, 32306, USA. E-mail: fliu@fsu.edu*
[b] *Institute of Molecular Biophysics, Florida State University, 91 Chieftan Way, Tallahassee, Florida, 32306, USA*

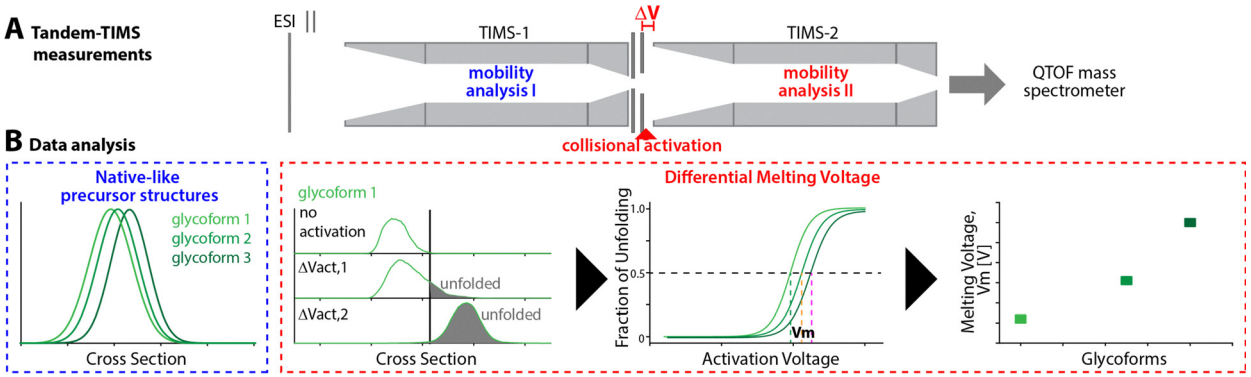

Fig. 1 Schematic overview of differential melting voltage workflow in a Tandem-Trapped Ion Mobility Spectrometry (Tandem-TIMS) instrument for elucidating the stability of distinct protein glycoforms. (A) Tandem-TIMS comprises two TIMS devices integrated within a QTOF mass spectrometer. To preserve native-like protein structures, ions are electrosprayed and analysed in TIMS-1 under native conditions. Ions are then activated (ΔV) in the interface region between TIMS-1 and TIMS-2 before undergoing a second mobility analysis in TIMS-2. (B) The data analysis workflow includes the following steps: (1) cross sections obtained under native conditions are compared with those calculated for X-ray or NMR structures to confirm the native-like state of precursor ions; (2) the fraction of unfolded conformation (highlighted as shaded areas) are extracted from cross section distributions at each activation voltage; (3) fraction of unfolded conformation is plotted as a function of activation voltage for individual glycoforms; and (4) the melting voltage (V_m), defined as the voltage at which half of the population is in the unfolded state, are compared across different glycoforms.

this method evaluates the energy associated with the transition of a protein from its native (folded) to unfolded state. This approach leverages the ability of Tandem-TIMS (Fig. 1A) to (1) retain proteins in a solution-like conformation in TIMS-1, (2) unfold the protein by applying an activation voltage in the interface between TIMS-1 and TIMS-2, and (3) determine the degree of unfolding of the activated protein *via* mobility analysis in TIMS-2. The data analysis involves several steps (Fig. 1B). First, the cross sections of protein glycoforms are determined in TIMS-1 and compared to the cross section values calculated from the X-ray or NMR structures to ensure that native-like conformations are retained. In the second step, the fraction of unfolded conformation is estimated for a range of activation voltages for each protein glycoform. Third, the fraction of the unfolded conformation is plotted as a function of the activation voltage. Finally, the melting voltage (V_m), defined as the voltage at which half of the protein is in the unfolded state, is extracted for each glycoform from the plot. Comparing the melting voltages across protein glycoforms is expected to provide insights into how variations in glycan sequence and structure contribute to the overall stability of the protein.

In the following, we applied the differential melting voltage approach to investigate the stability of distinct Ribonuclease B (RNase B) glycoforms. RNase B is an enzyme with one *N*-glycosylated site at Asn34, comprising five glycoforms with various numbers of mannose residues in the attached glycan.[19,20] RNase B has a non-glycosylated counterpart, RNase A. Although DSC and DSF methods have been used to analyze RNase B ensemble and partly deglycosylated RNase B in solution,[19–22] the stability of the five distinct glycoforms ($Man_{5-9}GlcNAc_2$-RNase) has not yet been resolved.

To apply our differential melting voltage approach, we first assessed the ability of Tandem-TIMS to retain intact RNase B glycoforms. To this end, RNase B was electrosprayed into the Tandem-TIMS instrument under native conditions as described.[12,14] Detailed experimental procedures are provided in Section S1 of the SI. The resulting mass spectrum is dominated by charge states 7+ to 9+ (Fig. S2, SI). Each charge state comprises five distinct RNase B glycoforms ($Man_{5-9}GlcNAc_2$-RNase), consistent with previous solution-phase and gas-phase reports.[19,21,22] The observed relative proportions of the glycoforms are consistent with the work by Dwek and coworkers using direct and indirect analysis of glycoforms (Table S1, SI).[19] Further, our data show elevated abundances of the glycoforms with greater mannose content ($Man_{7-9}GlcNAc_2$-RNase) compared to the gas phase proteolysis[21] and intact methods.[22] This observation suggests less fragmentation of larger glycan subunits during ionization and ion mobility/mass spectrometry measurements in Tandem-TIMS. These findings align well with earlier work from our laboratory,[14,17,23,24] highlighting the capability of Tandem-TIMS to preserve intact protein structures by minimizing ion heating.

To assess if the RNase B glycoforms retain native-like conformations in Tandem-TIMS, we compared the experimentally measured cross sections with those derived from the X-ray structure. The measured cross sections for intact glycoforms with charge states 7+ and 8+ are plotted in Fig. 2A. We contrasted the experimental cross sections with those calculated for the representative three-dimensional models of RNase B glycoforms, generated by integrating the X-ray structure of RNase B[25] (PDB ID: 1RBB) with $Man_{5-9}GlcNAc_2$ glycans (Fig. 2B and Fig. S4, SI). The experimental cross section values are lower than those estimated for the 3D models by ~10%, which suggests a compaction of RNase B glycoforms in the absence of solvent, as commonly observed in native mass spectrometry.[26,27] Overall, our data demonstrate that intact, native-like structures of RNase B glycoforms are preserved in Tandem-TIMS.

We then determined the melting voltage of individual RNase B glycoforms by subjecting the glycoforms to DC voltages ranging from 5 V to 60 V between TIMS-1 and TIMS-2 (Fig. 1A). Changes

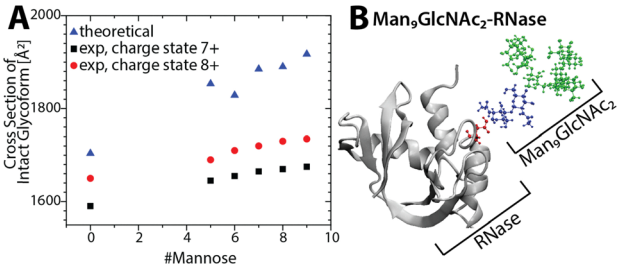

Fig. 2 Native mass spectrometry analysis of distinct RNase B glycoforms by Tandem-TIMS. (A) The cross section increases with the number of mannose residues for charge states 7+ (black rectangles) and 8+ (red dots). These trends are consistent with theoretical cross section values calculated for the X-ray structure (PDB ID: 1RBB) of RNase B (blue triangles). (B) A representative three-dimensional structure of $Man_{9}GlcNAc_{2}$-RNase.

in the cross section are probed by mobility analysis in TIMS-2. The fraction of the unfolded conformation is identified for increasing activation voltages (Fig. 1B).

We evaluated the consistency between the stability behaviour of RNase B observed in Tandem-TIMS and solution-phase studies. The population of unfolded conformations is quantified for each glycoform with charge state 8+ from the cross section distributions (Fig. S5, SI) and plotted as a function of activation voltage (Fig. 3A). We emphasize two consistent aspects of RNase B unfolding behaviour observed in our approach and solution phase studies. First, the melting curves exhibit a single, sharp sigmoidal increase (Fig. 3A), indicating a single transition from native-like to unfolded conformation. This observation is consistent with the differential scanning calorimetry and fluorimetry data of the RNase B ensemble and partly deglycosylated RNase B species, respectively.[28,29] Second, our data showcase higher melting voltages of RNase B glycoforms than its unglycosylated counterpart, RNase A. This trend aligns with solution-phase studies, which report higher thermal stability of RNase B ensemble compared to RNase A.[28–30] Both findings emphasize the consistency between differential melting voltage data and the solution phase reports.

As mentioned above, solution-based methodologies are limited in their ability to resolve the stability of individual RNase B glycoforms due to the difficulty of separating closely related glycoforms in solution. For instance, a DSC study reported the thermal unfolding profiles for RNase B ensemble and two partly deglycosylated forms of RNase B ($Man_{1}GlcNAc_{2}$ and GlcNAc).[29] However, to date, no studies have reported on the relative stability of the five distinct RNase B glycoforms.

In contrast, the differential melting voltage approach described above characterises the relative unfolding stability of individual RNase B glycoforms. Accordingly, our approach probes the influence of molecular mass and shape/size on glycoform stability by correlating the melting voltage of individual glycoform to the glycan mass and the intact glycoform cross section (Fig. 3B and C). The melting voltage increases with the number of mannose residues in the attached glycan, suggesting a corresponding increase in the activation energy barrier for unfolding. Strikingly, both diagrams show a non-linear relationship between the melting voltage of RNase B

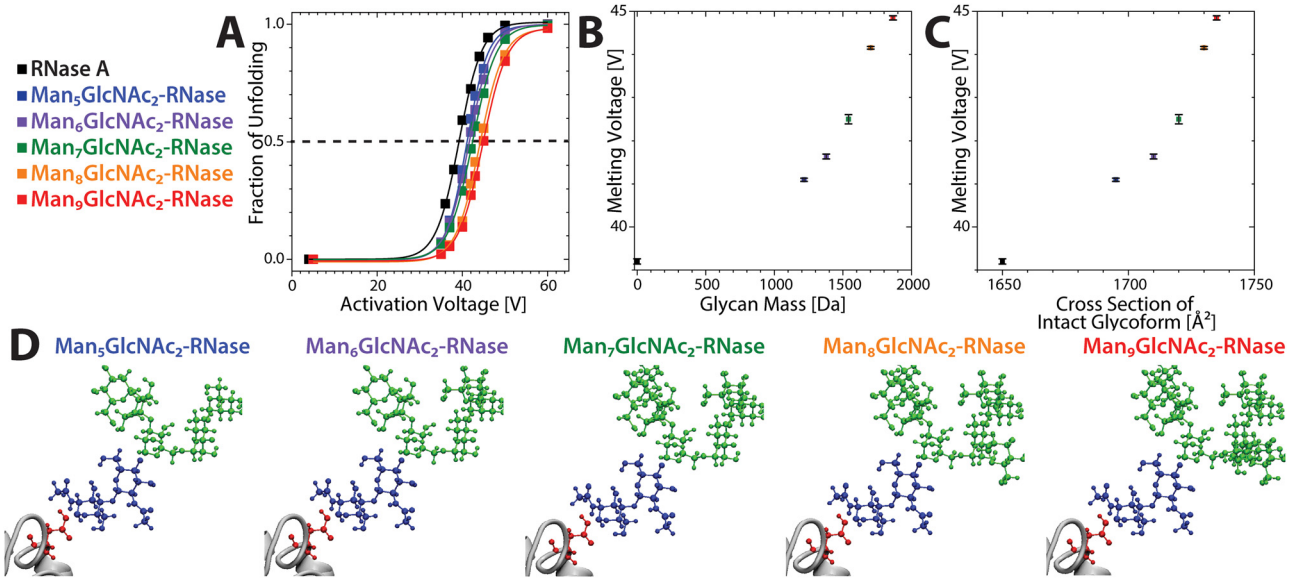

Fig. 3 Differential melting voltage analysis reveals that glycan structure contributes to the overall stability of RNase B glycoforms. (A) The fraction of unfolded conformations for distinct RNase B glycoforms ($Man_{5-9}GlcNAc_{2}$-RNase) with charge state 8+ is shown as a function of accelerating DC voltage (5–60 V). (B) and (C) Melting voltages of various RNase B glycoforms are plotted as a function of glycan mass and intact glycoform cross section. Two subgroups of RNase B glycoforms are revealed. The first subgroup comprises lower mannose-containing glycoforms ($Man_{5-7}GlcNAc_{2}$-RNase), exhibits a modest increase in the melting voltage per additional mannose residue. The second subgroup, which has higher number of mannoses ($Man_{8-9}GlcNAc_{2}$-RNase), display a higher increase in the melting voltage per mannose residue. (D) Representative 3D structures of the glycan moiety attached to the RNase scaffold illustrate additional sugar residues in $Man_{8-9}GlcNAc_{2}$, which possibly contribute to enhanced stability of the enzyme through greater steric interactions.

glycoforms and either the glycan mass or the intact glycoform cross section. The diagrams further suggest that RNase B glycoforms can be classified into two different subgroups (Fig. 3B and C). The first subgroup, comprising lower mannose-containing glycoforms (Man5–7), exhibits a modest increase in melting voltages compared to the second subgroup (Man8–9).

These findings indicate that structural aspects of the attached glycan, beyond mass and shape, play an essential role in protein stability. The bulkiness of additional mannose units in Man8–9 (Fig. 3D) most probably adds to the elevated steric hindrance, which contributes to enhanced protein stability. Taken together, the differential melting voltage analysis indicates that the glycan structure is a significant determinant of overall protein stability.

Conclusions

The differential melting voltage (DMV) method evaluates the unfolding profiles generated by collisional activation measurements using a single, quantifiable metric for each glycoform. This enables (1) direct comparison of stability between various glycoforms, and (2) direct correlation between stability and molecular properties, such as mass, intact protein size, or the glycan structure.

Applying this approach to RNase B glycoforms, we observed: (1) glycosylation contributes to the overall protein stability, (2) structural aspects of the attached glycan, beyond mass and shape, are critical to the stability of the intact protein. Currently, the DMV method is limited in its ability to distinguish distinct structural isomers of individual glycoforms.

We contextualize our findings within the broader framework of glycoproteins stability. Previous studies using scanning calorimetry/fluorimetry and molecular dynamics simulations demonstrated that glycosylation enhances protein stability by destabilizing the unfolded state through steric hindrance imposed by the bulky glycan units.[31,32] Consistent with these studies, our DMV data indicate an increase in unfolding stability of RNase B glycoforms with a greater steric effect of the attached glycan. Given the ability of Tandem-TIMS to perform non-ensemble, conformational-specific measurements,[18] this finding highlights the potential of the differential melting voltage approach for resolving subtle structural and stability differences among closely related protein glycoforms. As such, this study underscores the utility of tandem-ion mobility coupled to tandem-mass spectrometry in analysing complex, heterogeneous biological systems.

Conflicts of interest

There are no conflicts to declare.

Data availability

The data supporting this article are found in the SI. Supplementary information: Materials and Methods, Mass and ion mobility spectra, Cross section calculations, Representative structural models. See DOI: https://doi.org/10.1039/d5cb00127g

Acknowledgements

This work is supported by the National Science Foundation (CHE 2305173) and the National Institutes of Health (R01GM135682).

Notes and references

1 R. Apweiler, *Biochim. Biophys. Acta, Gen. Subj.*, 1999, **1473**, 4–8.
2 H. J. An, J. W. Froehlich and C. B. Lebrilla, *Curr. Opin. Chem. Biol.*, 2009, **13**, 421–426.
3 M. Molinari, *Nat. Chem. Biol.*, 2007, **3**, 313–320.
4 R. J. Woods, *Chem. Rev.*, 2018, **118**, 8005–8024.
5 G. P. Subedi and A. W. Barb, *Structure*, 2015, **23**, 1573–1583.
6 R. Wada, M. Matsui and N. Kawasaki, *mAbs*, 2019, **11**, 350–372.
7 T. Wohlschlager, K. Scheffler, I. C. Forstenlehner, W. Skala, S. Senn, E. Damoc, J. Holzmann and C. G. Huber, *Nat. Commun.*, 2018, **9**, 1713.
8 Y. Tian and B. T. Ruotolo, *Int. J. Mass Spectrom.*, 2018, **425**, 1–9.
9 W. Hoffmann, J. Hofmann and K. Pagel, *J. Am. Soc. Mass Spectrom.*, 2014, **25**, 471–479.
10 M. Guttman and K. K. Lee, *Anal. Chem.*, 2016, **88**, 5212–5217.
11 Y. Tian, L. Han, A. C. Buckner and B. T. Ruotolo, *Anal. Chem.*, 2015, **87**, 11509–11515.
12 F. C. Liu, M. E. Ridgeway, M. A. Park and C. Bleiholder, *Analyst*, 2018, **143**, 2249–2258.
13 F. C. Liu, M. E. Ridgeway, M. A. Park and C. Bleiholder, *Analyst*, 2022, **147**, 2317–2337.
14 F. C. Liu, T. C. Cropley, M. E. Ridgeway, M. A. Park and C. Bleiholder, *Anal. Chem.*, 2020, **92**, 4459–4467.
15 F. C. Liu, S. R. Kirk, K. A. Caldwell, T. Pedrete, F. Meier and C. Bleiholder, *Anal. Chem.*, 2022, **94**, 8146–8155.
16 J. Lee, M. Chai and C. Bleiholder, *Anal. Chem.*, 2022, **95**, 747–757.
17 T. C. Cropley, F. C. Liu, M. Chai, M. F. Bush and C. Bleiholder, *J. Am. Chem. Soc.*, 2024, 11115–11125.
18 F. C. Liu, J. Lee, T. Pedrete, E. M. Panczyk, S. Pengelley and C. Bleiholder, *Chem. Commun.*, 2024, **60**, 10740–10743.
19 M. Rudd, I. G. Scragg, E. Coghill and A. Dwek, *Glycoconjugate J.*, 1992, **9**, 86–91.
20 D. Fu, L. Chen and R. A. O'Neill, *Carbohydr. Res.*, 1994, **261**, 173–186.
21 S. Hua, C. C. Nwosu, J. S. Strum, R. R. Seipert, H. J. An, A. M. Zivkovic, J. B. German and C. B. Lebrilla, *Anal. Bioanal. Chem.*, 2012, **403**, 1291–1302.
22 V. K. James, A. A. M. Van Der Zon, E. E. Escobar, S. D. Dunham, A. F. G. Gargano and J. S. Brodbelt, *J. Proteome Res.*, 2024, **23**, 4684–4693.
23 F. C. Liu, S. R. Kirk and C. Bleiholder, *Analyst*, 2016, **141**, 3722–3730.

24 C. Bleiholder, F. C. Liu and M. Chai, *Anal. Chem.*, 2020, **92**, 16329–16333.
25 R. L. Williams, S. M. Greene and A. McPherson, *J. Biol. Chem.*, 1987, **262**, 16020–16031.
26 B. T. Ruotolo, K. Giles, I. Campuzano, A. M. Sandercock, R. H. Bateman and C. V. Robinson, *Science*, 2005, **310**, 1658–1661.
27 Z. Hall, A. Politis, M. F. Bush, L. J. Smith and C. V. Robinson, *J. Am. Chem. Soc.*, 2012, **134**, 3429–3438.
28 P. Del Vecchio, F. Catanzano, B. De Paola and G. Barone, *J. Therm. Anal. Calorim.*, 2000, **61**, 363–368.
29 W. Pfeil, *Thermochim. Acta*, 2002, **382**, 169–174.
30 U. Arnold and R. Ulbrich-Hofmann, *Biochemistry*, 1997, **36**, 2166–2172.
31 R. J. Solá, J. A. Rodríguez-Martínez and K. Griebenow, *Cell. Mol. Life Sci.*, 2007, **64**, 2133–2152.
32 D. Shental-Bechor and Y. Levy, *Proc. Natl. Acad. Sci. U. S. A.*, 2008, **105**, 8256–8261.